Optimal Battery Sizing for 24-hour Critical Load Support in a Building-level Microgrid

Jeremy Lytle[1], Alan Fung[1], Falon Attai[2], Livio Nichilo[2]
[1]Ryerson University, Toronto, Canada
[2]Internat Energy Solutions, Toronto, Canada

Abstract

The increasing frequency of extreme weather events and projections of future electricity demand pose substantial operational threat to aging electricity infrastructure. Microgrids are becoming an attractive method of providing energy independence and resilience in this environment of uncertainty. The present analysis evaluates a design-phase microgrid proposed for implementation in Toronto against the stipulated resiliency target; to provide 24 hours of critical load support in an extended outage. An energy reservoir battery model is developed in python with inputs from Helioscope. Hourly outage simulations are conducted to evaluate trends in duration of critical load support. An economically optimal battery range is identified by considering the incremental cost of storage capacity as a function of the probability of achieving the target. The model is then extrapolated to Calgary, Vancouver and Los Angeles to explore variability in the results according to consistency of photovoltaic yield. A sensitivity analysis identifies linear dependencies between the optimal storage capacity and mean daily production and consumption within the microgrid. A multiple linear regression predictive model is thus proposed to approximate the battery capacity corresponding to 95% probability of success as a function of these early stage design variables.

Introduction

A microgrid can be described as a localized network of electrical loads and power sources with the capacity to function independently or in conjunction with a larger grid system (Tsikalakis & Hatziargyriou, 2011). The decentralized nature of microgrids enable rapid implementation of electrical infrastructure in developing countries where broader grid infrastructure has limited reach (Zimmerle & Manning, 2017). In more developed countries, microgrids provide energy independence from national electricity distributers, which can result in economic benefits as well as resilience to extreme weather events and infrastructure failures. One such system of global noteworthiness is the Sendai Microgrid. This system has been internationally recognized for its resilience in supplying power to its load base despite the occurrence of the Great East Japan Earthquake that devastated local district energy supply (Hirose, Shimakage, Reilly, & Irie, 2013).

The growing interest in microgrid technology necessitates a broader understanding of design implications and development of reliable tools. Some commercial design tools exist for modelling a variety of aspects of microgrid performance. HOMER is one such tool which utilizes a variety of built in component models to construct a microgrid and simulate annual energy performance. HOMER is generally employed to conduct sizing optimization with net present cost as the objective function (Kumar & Bhimasingu, 2014), and has the capacity to consider sensitivity in input variables. PSCAD is a similar design tool that forgoes economic optimization in the interest of detailed electrical design and control analysis (Ahamed, Dissanayake, De Silva, Kumara, & Lidula, 2016). Both of these design tools lack the interactive functionality to evaluate outage performance as desired by the present work.

Sandia National Laboratories has twice reviewed the state of the art in energy storage modeling for control and grid integration applications. (Byrne, Nguyen, Copp, Chalamala, & Gyuk, 2017), (Rosewater, Copp, Nguyen, Byrne, & Santoso, 2019). The surveyed body of state-of-charge (SoC) modeling approaches have been categorized in accordance with the units used to define available charge. Energy reservoir models (ERMs) consider efficiency-rated energy transactions at a high level and lack the granularity to consider chemical or electrical dynamics. These models have the lowest accuracy of any category and also the lowest computational load. Charge reservoir models (CRMs) account for SoC in units of ampere-hours (Ah). This approach utilizes an equivalent circuit model to approximate the electrical dynamics of charge and discharge. Circuit models are customizable to approximate a variety of battery technologies, and accuracy is increased relative to the ERM approach at the cost of computational complexity. The third category encompasses concentration-based models, which are highly technology specific and seek to model detailed battery chemistry. This approach has the greatest accuracy potential, requiring a high level of detail about the cell design and a heavy computational load.

In the present analysis the energy reservoir modelling approach has been selected. This type of model is best suited to the time scale of the intended simulation, allowing for a high-level estimate of the state of charge on an annual basis. The ERM approach has been used previously in building-level energy storage simulations of a similar variety (Leadbetter & Swan, 2012). This approach is also best suited for comparative analysis of a variety of battery technologies.

Background

Project Objectives & Scope

The analysis begins in the interest of optimizing battery capacity in a subject building microgrid in Toronto. The primary design intent of the subject microgrid is to provide emergency back-up power to the building. The system also aims to provide a degree of peak load shedding, although the economic benefits of this are not significant. The main performance criterion is thus to provide a minimum 24-hours of critical load support in the event of an extended outage compromising both electricity and natural gas supply.

Previous approaches have endeavored to address this goal via optimal management of controllable loads (Cui & Liu, 2016). In the present approach, load control is not considered, rather the problem is addressed from the perspective of optimal storage system design.

Microgrid Architecture & Specifications

The subject microgrid system is located in Toronto, ON and contains the elements presented in Table 1.

Table 1: Microgrid system specifications

Peak Building Load (kW)	75
Peak Critical Load (kW)	22
Peak EV Charging Load (kW)	14.8
PV Nameplate Power (kW)	31.1
Max Generator Power (kW)	75
Rated Battery Capacity (kWh)	324
Battery Output Power (kW)	30

In order to simplify operations and compliance, the subject microgrid is not designed to be bi-directionally grid interactive. The building's critical load circuit is decoupled from the main electricity supply and supported solely by the microgrid, which accepts grid electricity as an input.

The solar photovoltaic (PV) system is spatially constrained by the building's rooftop area. Within this constraint production capacity is maximized at a tilt angle of 10° due to limited self-shading and maximized ground-coverage ratio.

The natural gas generator is reserved for full building load support in emergency operation and thus falls outside the present scope of analysis. Main variables considered are storage capacity, discharge control, and related economics.

Modelling Methodology

A three-tiered modeling framework is implemented using Helioscope and Python, as presented in Figure 2. The objective of the framework is to approximate the hourly SoC profile within the microgrid and simulate outages within that profile, in order to produce a dataset of load support duration that can be statistically analyzed. Individual elements of the framework are described in the following sections.

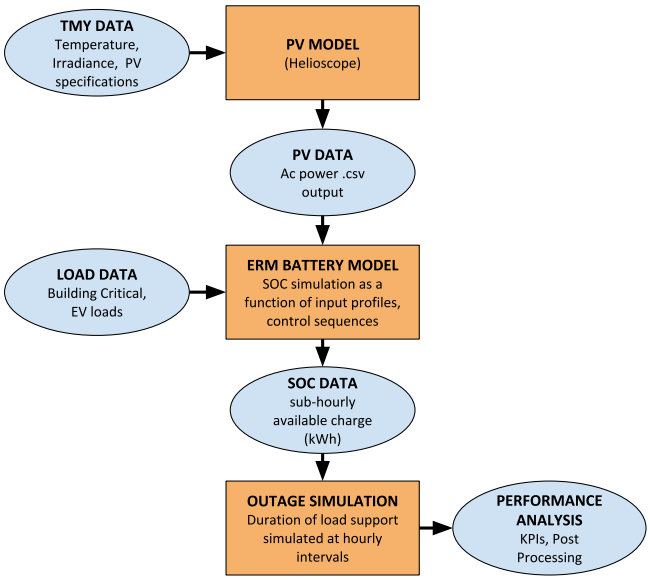

Figure 1: System Modelling Framework

Critical Load Profiles

Daily load profiles for both the winter and summer conditions were generated based on the residential building typology and supported by detailed energy audits. Load profiles are extrapolated over an annual term at hourly resolution in coordination with production data. A sample plot of the winter load data is presented in Figure 2.

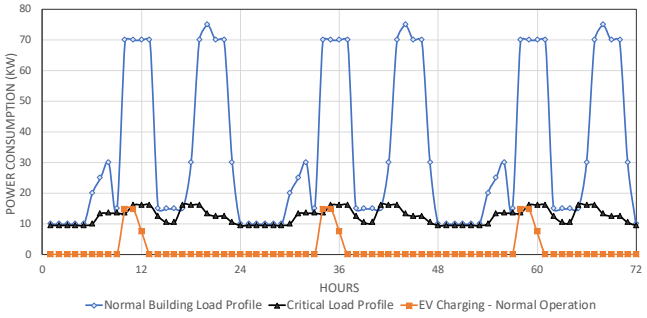

Figure 2: Sample winter condition load profiles

Winter and summer conditions vary by a daily magnitude of about 7% due to the inclusion of small seasonal loads. In the annual profile, summer condition is employed from April 1st to September 30th and winter condition from October 1st to

March 31st. No considerations are made for a transition period or shoulder season profile. In future it is proposed that this can be improved with more representative input from a building energy model or a stochastic approach.

Photovoltaic Simulation

The Helioscope modelling engine has been validated to within 1% of industry standard PVSyst (BEW Engineering, 2013), and thus is considered an adequate tool for this study. Since the Helioscope model includes the selected inverter for the system, the simulated AC power output is extracted for battery model input. This dataset has an hourly resolution and does not include the grid connectivity losses applied to Helioscope end-use output. Source data for the PV simulation is a local model based TMY weather file from Meteonorm, with 10km resolution (Meteotest, 2019).

The modelled system is equipped with two 15kW inverters resulting in a load ratio of 1.04. Modules are positioned in landscape orientation with a tilt angle of 10° and azimuth of 163°. A constant monthly soiling factor of 2% is applied to the simulation, which neglects additional losses and reliability implications due to snowfall events (Andrews, Pollard, & Pearce, 2013).

Control Sequence

The desired functionality of the energy storage system (ESS) is to accept charge during the same portion of the day for which it is supplying the building's critical load and EV chargers. Given that this simultaneous operation is not possible at the scale of a single cell, an alternate solution must be derived. In the context of the model, the ESS is assumed to be separated into two cell blocks, so at any given time one block may be charging while the other discharges.

A double-pole, triple-throw switching configuration is employed to dictate the available operational states of the system as presented in Figure 3.

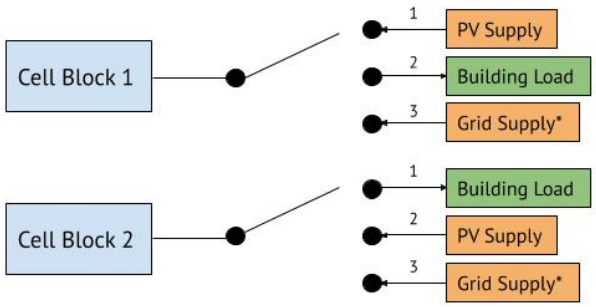

Figure 3: Assumed switching configuration used to define operational states 1-3.

State 3 represents the off-peak operation, while state 1 and 2 represent on-peak operation. Switching between states 1 and 2 is triggered by either cell block reaching its minimum or maximum state of charge.

The technical complexities associated with the control of such an implementation are recognized, however beyond the scope of this analysis. It is simply assumed that the desired functionality of the system will ultimately be achieved resulting in a comparable overall energy flow to the modelled configuration.

Energy Reservoir Battery Model

Rosewater et al. (2019) define Equation 1 as the governing formula for an energy reservoir SoC model:

$$Q_{cap}\frac{\partial \varsigma}{\partial t} = \eta_{RT}p^{+} + p^{-} + p_{sd} \quad (1)$$

where Q_{cap} is the storage capacity in kWh, ς is the fractional SoC, η_{RT} is the ESS round trip energy efficiency, p^{+} is the charge power, p^{-} is the discharge power and p_{sd} is the self-discharge power, in kW.

In accordance with the ERM approach, current dependent efficiency fluctuation is simply accounted for with an average efficiency value. Due to lack of operational data from the manufacturer, self-discharge power and internal conditioning loads are neglected in this application.

The storage efficiency is taken to be 90%, and inverter efficiency is taken at an average of 96%. This results in a round trip conversion efficiency of 83%, in accordance with Equation 2, which is in agreement with published physics-based models for stationary lithium ion storage technology (Schimpe, et al., 2018).

$$\eta_{RT} = \eta_{inv} \cdot \eta_{storage} \cdot \eta_{inv} \quad (2)$$

Accounting for finite timesteps, and separating the round-trip efficiency into components, Equation 1 can be interpreted as follows, during on-peak operation:

$$\varsigma_i = \varsigma_{i-1} + \frac{E_{PV_i}\cdot\eta_{inv}\cdot\eta_{storage}}{Q_{cap}} - \frac{L_{crit_i}+L_{EV_i}}{\eta_{inv}\cdot Q_{cap}} \quad (3)$$

where E_{PV} is the quantity of energy supplied to the ESS by the PV system over timestep i in kWh, L_{crit} and L_{EV} are the quantities of energy consumed from the ESS over timestep i, by the critical load and EV chargers, respectively. Q_{cap} in this application refers to the rated capacity of the cell block upon which the loads are acting.

During off-peak operation, while the SoC remains below 100%, the model is governed according to Equation 4:

$$\varsigma_i = \varsigma_{i-1} + \frac{E_{grid_i}\cdot\eta_{inv}\cdot\eta_{storage}}{Q_{cap}} \quad (4)$$

where E_{grid} is the quantity of energy supplied to the ESS by the electric utility over timestep i in kWh. In this application, grid supply is governed by the limiting current of the circuit breaker, which allows for a constant supply of 38.4 kW, under safe operation.

SoC calculations are evaluated at 15-minute intervals and thus apply 25% of the hourly quantity of energy at each interval. The sub-hourly approach ensures that the minimum and maximum SoC thresholds can be honoured to a reasonable degree of precision without falsely correcting SoC values at edge cases, which would result in unaccounted quantities of energy.

Outage Simulation

Once the annual SoC profile is obtained, the outage performance can be examined. In order to do so an array of outage hours is generated, representing hours within the year when an outage is initiated. At each outage hour, the corresponding state of charge undergoes an ERM simulation at 15-minute intervals governed by Equation 3 until the rated battery capacity is diminished. Electric vehicle charging loads are omitted from outage operation. The duration of discharge is tracked for the entire outage dataset and compiled for further analysis.

Based on the unpredictable nature of power outages and variability of PV supply throughout the year, a thorough sampling of the SoC profile is required to produce a reliable dataset of outage performance. Ultimately the outage model is expanded to sample hourly throughout the year to achieve the necessary level of repeatability. Although the key design scenarios are concentrated around the lowest irradiance days, a full year simulation is merited to provide accurate hourly SoC estimations as well as contextualized probability metrics.

Performance Indicators

The main performance indicator of concern is the probability of success in achieving the duration target. This is denoted *P(s)* and can be approximated as the ratio of outage simulations achieving a 24-hour duration to the total number of outages. Mean and minimum values of the discharge duration dataset are also calculated for analysis.

Photovoltaic (PV) utilization is defined as the ratio of PV energy delivered from the microgrid to the total energy produced by the array. This term provides an overall measure of system efficiency as a function of battery technology and control intervention.

Model Results

Simulating the initial design case (324 kWh battery, 40% minimum SoC) yields the performance indicators summarized in Table 2. An expanded design space is subsequently explored in search of improved performance

Table 2:Initial design simulation results.

Success Probability (%)	PV Utilization (%)	Mean Duration (hrs)	Minimum Duration (hrs)
72.03%	83.14%	30.45	11.5

Effect of Discharge Limit

To investigate the potential effect on system performance a variety of minimum state of charge limits are simulated ranging from 30%-90% at 10% intervals. Results are summarized in Figure 4.

The results indicate a positive correlation between the success probability and outage durations and an increasing minimum charge threshold. This can be expected, as the minimum outage durations will occur when the battery is at a minimum state of charge. Increasing this minimum allows for longer outage duration in the worst-case scenario. The contrary effect is that PV utilization, represented by the dashed line in Figure 4, decreases with increasing SoC threshold. This is a function of additional demanded grid energy to maintain a higher storage capacity, which comprises the systems effectiveness in peak load shedding.

It can also be observed from Figure 4 that the minimum SoC limit has marginal effect on the mean duration (~15% change) in comparison to the minimum duration (~90% change). This is a logical outcome as the majority of outage simulations are initiated at an SoC much greater than the minimum and are thus unaffected.

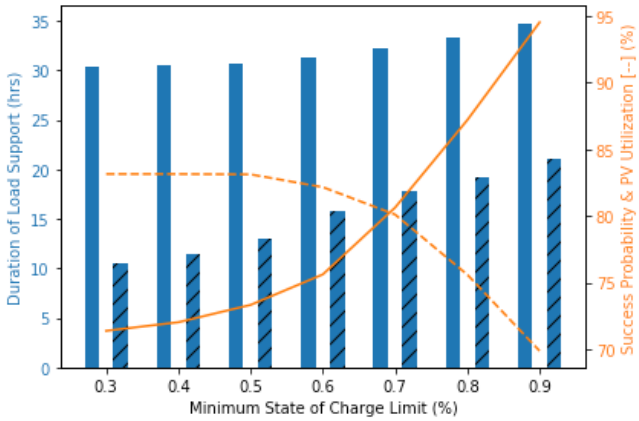

Figure 4:Success probability (solid line), PV utilization (dashed line), mean duration (solid bar) and minimum duration (hashed bar) as a function of minimum SoC limit.

Effect of Battery Capacity

Battery sizes in the range of 30%-170% of the initial design state are simulated at the initial minimum SoC threshold of 40% to showcase the overall trends. Results are presented in Figure 5.

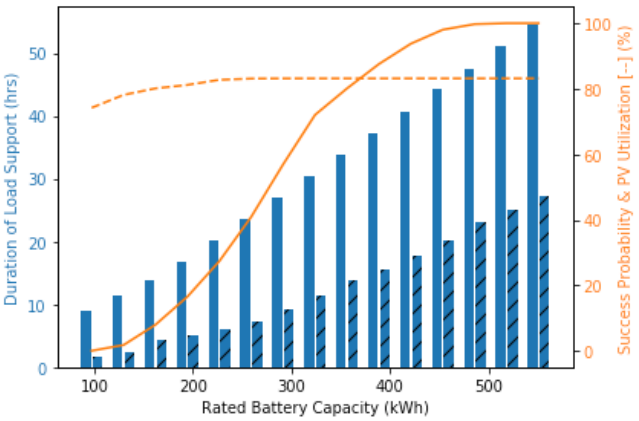

Figure 5:Success probability (solid line), PV utilization (dashed line), mean duration (solid bar) and minimum duration (hashed bar) as a function of battery capacity.

Interestingly, the success probability exhibits a varying slope with a steep ascent from roughly 20%-80% and

shallower conditions at the edge cases. It is hypothesized that this trend relates to the distribution of daily photovoltaic yield throughout the typical year in Toronto; a notion explored in greater detail in the sensitivity analysis section.

Figure 6 presents a surface plot of the success probability for the system encompassing the entire considered design spaces for both the storage capacity and minimum SoC threshold. The mechanism present is in accordance with expectations based on the Figures 4 & 5. The overall shape of the plot is predominantly governed by the inflecting curve proportional to battery capacity with some minor, yet noteworthy influence from the SoC threshold.

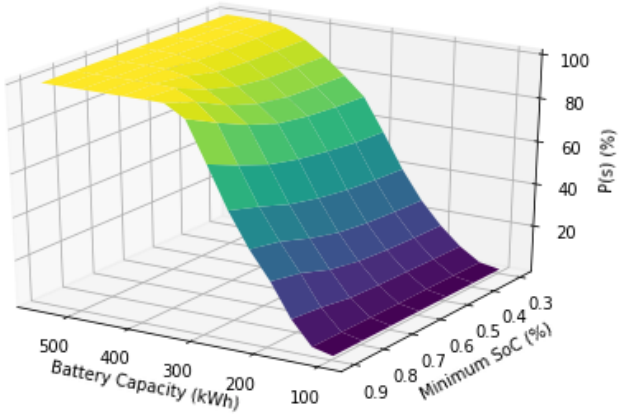

Figure 6: Success probability of considered design space.

Economic Considerations

From the trends exhibited in Figures 4-6, two economic consequences can be deduced. First, the incremental improvement in success rate with increasing SoC limit can be realized without an increase in capital cost. In this sense, the SoC limit provides free optimization capacity, although codependent return mechanisms such as PV utilization and peak load shedding must be considered .

Secondly, the inflection of the surface in the battery capacity axis indicates that there are diminishing returns to battery capacity investment in the range approaching 100% success. To determine the point offering the greatest value, the cost of storage may be divided by its corresponding success probability. This produces a measure of the incremental cost of success probability, defined in units of dollars per percentage. This measure is applied to the considered design space in Figure 7. The results present a local minimum indicating an economic optimum in this context. A more comprehensive economic analysis ought to consider the value of resilience, which relates to the avoided costs of outages, thus providing a more quantifiable measure of payback than can be realized with reference to probability.

Battery capital costs are evaluated at a rate of $594 CAD/kWh, in accordance with supplier estimates. It should be noted that this price applies to the ESS installed capacity, which exceeds the rated capacity by 20% due to the reserve capacity which cannot be discharged.

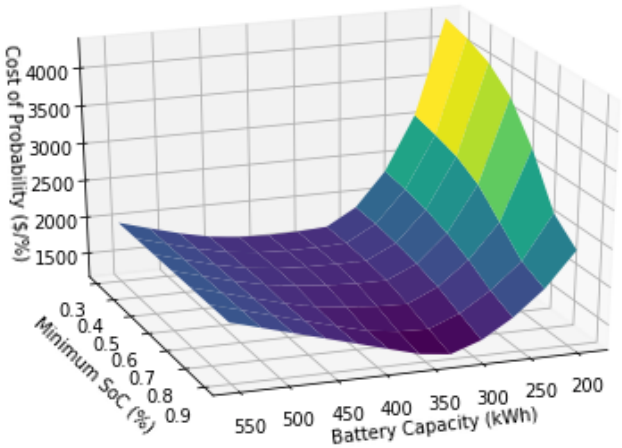

Figure 7: Incremental cost of success probability over considered design space.

A detailed inspection of the data presented in Figures 6 & 7 allows the microgrid designer to select an optimal battery capacity based on the informed compromise between success probability and corresponding incremental cost. Figure 7 presents relatively uniform minima extending roughly between capacities of 324 kWh to 425kWh. At the larger extent of this range, success probabilities in the range of 85%-100% are achievable dependent upon the minimum SoC threshold.

Sensitivity Analysis

A sensitivity analysis is undertaken to generate further insight into the trends observed in the simulation results. Minimum SoC is held constant at 60% in order to isolate variables relating to PV production and critical load.

An additional performance indicator, denoted P95 battery capacity, is introduced as the minimum battery capacity in kWh that meets or exceeds 95% success probability. This indicator represents a design with sufficient performance to meet the design goal, recognizing that there exists a range of unlikely but possible circumstances for which the goal will not be met. This notion of designing for less than 100% of possible conditions is common in HVAC practice, which also relies on weather data for design conditions. It is also supported by Zimmerle and Manning (2017) who observed in their study of microgrid sizing for rural applications that it is sub-optimal from an economic perspective to design for 100% reliability.

Consistency of Photovoltaic Resource

To explore the effect related to distribution of daily photovoltaic yield on optimal system sizing, the model is evaluated at three additional locations, with all system parameters otherwise held constant. Locations are selected for their climatic and latitudinal differences as well as relevance to the microgrid industry.

The attribute of interest can be visualized in a histogram of daily PV production, as depicted in Figure 8.

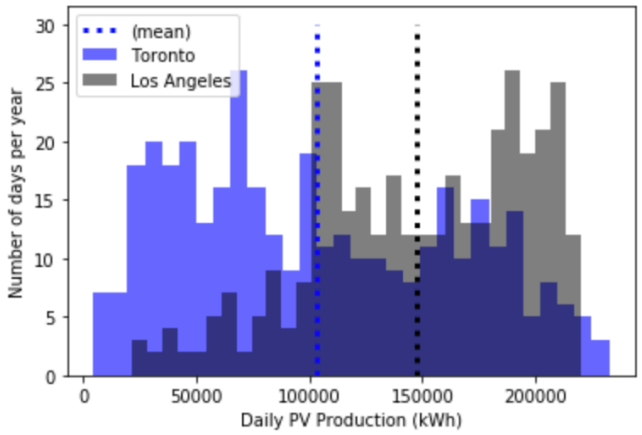

Figure 8: Histogram of daily PV production in Toronto and Los Angeles for the subject 31.1 kW system.

Due to its greater latitude, the Toronto resource exhibits a wider range of productivity, showcasing production days exceeding both the maximum and minimums present in Los Angeles. It can also be noted that the Los Angeles data is grouped rather symmetrically about its mean with a tail of low production days, contrary to the Toronto data which is widely dispersed with a prominent clustered of days below its mean. This characteristic of the data is theorized to have effect on optimal design proportions and thus must be quantified. For this purpose, the ratio of standard deviation to the mean (STDR) in a daily production dataset is assumed a sufficient approximator.

Details of the photovoltaic resource in each of the selected locations are summarized in Table 3. Table 4 presents the corresponding simulation results. Capacity and incremental cost differentials refer to the percent difference between the stated measures at the economic optimum and 95% success conditions.

Table 3: PV resource data at evaluated locations

Location	Specific Yield (kWh/kW)	Percent Difference	Mean Daily Production (kWh)	Standard Deviation (kWh)	Standard Deviation Ratio (%)
Toronto	1207	0.0%	103.3	59.9	58.0%
Calgary	1282	6.2%	109.7	59.4	54.1%
Vancouver	1091	-9.6%	92.6	60.6	65.4%
Los Angeles	1726	43.0%	147.7	47.7	32.3%

Table 4: Simulation results at evaluated locations

Location	Economic Optimum Capacity (kWh)	P(s) at Economic Optimum (%)	95% Capacity (kWh)	Capacity Differential (%)	Incremental Cost Differential (%)
Toronto	324	76.50%	421	29.94%	13.50%
Calgary	332	81.70%	421	26.81%	8.40%
Vancouver	340	78.10%	445	30.88%	7.43%
Los Angeles	284	82.70%	340	19.72%	4.00%

Trends in these results are generally aligned with expectations. Los Angeles, which exhibits the greatest mean production and least STDR requires the least battery capacity in both the optimum and 95% conditions. Conversely Vancouver, which is opposite in both measures, requires the greatest storage capacity in both conditions. Toronto and Calgary exhibit relatively similar production profiles and results. This analysis indicates that PV resource effects model output, however; does not allow for identification of the mechanism.

Production Dependency

To further investigate the effects of PV production, array size can be modulated. This outcome is approximated by post processing Helioscope data with a simple incremental multiplier. Although this approach neglects changes to electrical balance of system design that may occur at different system sizes, it is considered adequate for the purposes of the analysis.

At reasonable variances in array size, the economic optimum presented in Figure 7 no longer holds. As a result, the remainder of this analysis will focus on the P95 capacity as the dependent variable. This is also considered the measure of broader utility.

Figure 9 depicts the P95 battery capacities plotted for each location over a range of array sizes, quantified by mean daily production. The resultant trends indicate a negative linear correlation between production capacity and P95 storage capacity, for a given location. Examining trendline fits to data at each location, it can also be observed that there is an inverse correlation between slope and PV resource STDR. This is a logical outcome, as the distribution of the dataset scales with the mean. It can thus be reasoned that a magnitude variance in a sparser dataset would have less effect on the worst-case outage scenarios than a more concentrated dataset. The y-axis offset is also assumed to be a function of STDR, as discussed previously.

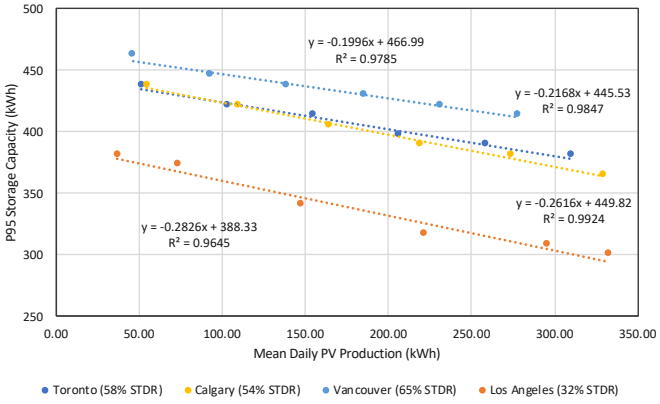

Figure 9: P95 battery capacity as a function of mean daily production at evaluated locations.

Consumption Dependency

Another microgrid characteristic of significance to modelled outcomes is the magnitude of daily consumption. This dependency is evaluated in a similar fashion to the production dependency by applying an incremental

multiplier to the critical and EV load profile data, such that the data is affected only in magnitude. A proportional multiplier is also applied to the simulated battery capacity range in order to maintain a compatible design space.

The observed relationship is a positive linear correlation between mean daily consumption and P95 battery capacity, as depicted in Figure 10.

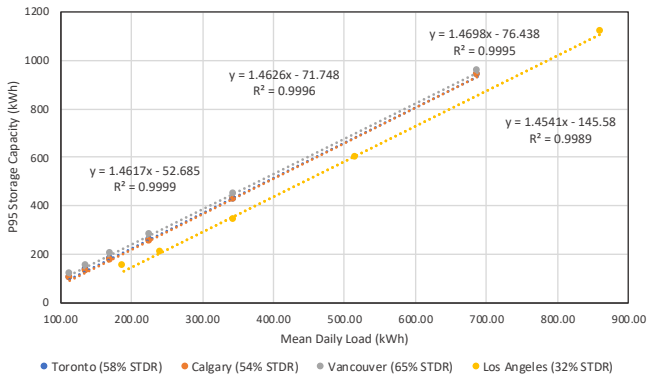

Figure 10: P95 battery capacity as a function of mean daily consumption at evaluated locations.

There is a slight offset in the y-axis between location which can likely be attributed to variance in magnitude of production. However, the offset is insignificant enough that the Toronto data points are eclipsed by the Calgary data in the plotted resolution. Trendlines exhibit nearly identical slopes between locations, which suggests a dependence on factors held constant in this analysis. Perhaps round-trip efficiency and hourly load profile distribution might be influencing variables.

It can also be noted that dependence on consumption is roughly 7 times stronger than the dependence on production, according the magnitude of slope coefficients. This can be expected as consumption is much more constant throughout the annual simulation, thus affecting duration of load support more directly.

Simplified Predictive Model

With the reported dependencies established, a multiple linear regression model (LRM) can be employed to approximate the P95 battery capacity as a function of mean daily PV production and mean daily load. This sort of simplified calculation is of value to the microgrid design community as it allows approximation of system requirements without detailed simulation work. The basic formula for such a model is described by Equation 5.

$$y = \beta_0 + \beta_1 x_1 + \beta_2 x_2 + \cdots + \beta_n x_n + \varepsilon \qquad (5)$$

Where y represents the dependent variable, β_0 represents the y-intercept, $\beta_{1\text{-}n}$ represent the slope coefficients for independent variables $x_{1\text{-}n}$ and ε represents model residuals.

Adapting Equation 5 to estimate P95 battery capacity in Toronto yields Equation 6:

$$Q_{P95} = 1.462 \cdot \bar{E}_{LD} - 0.218 \cdot \bar{E}_{PV} + C_0 \qquad (6)$$

where C_0 represents an offset coefficient inclusive of model residuals, 1.462 is an average of consumption dependent slope coefficients presented in Figure 10, -0.218 is the Toronto production dependent slope coefficient from Figure 9, and E_{PV} and E_{LD} are the daily mean PV production and load consumption, respectively. Mean values are calculated according to Equation 7:

$$\bar{E}_{LD} = \frac{\Sigma_0^{8760} E_{LD}}{n} \qquad (7)$$

where n represents to number of target duration periods in a year, in this case 365.

Offset coefficients are initially calibrated to the y-intercepts of production trendlines, and subsequently tuned to minimize percent root mean square error (%RMSE) once a body of predictions is developed. Mean average prediction error (MAPE) is also evaluated and is observed to minimize in coincidence with %RMSE.

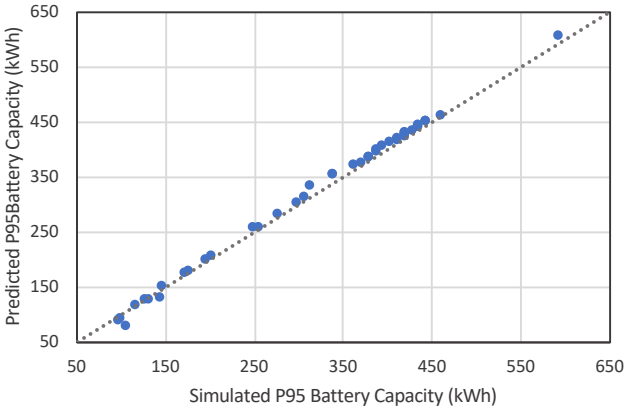

Figure 11: LRM predicted capacities vs simulated results, with dotted line representing y=x.

Model predictions are plotted against simulated results over the entire range of simulated conditions and locations in Figure 11. Table 5 summarizes the model coefficients and prediction error exhibited at each of the evaluated locations. MAPE is less than 1% for all locations except Los Angeles, which indicates good reliability in the model. However, it is expected that error is limited in this context as the model is only compared against the simulation results upon which it was built. A truer evaluation of the applicability of the model would test conditions outside the development group.

Table 5: Summary of model coefficients and resultant prediction error.

Location	PV STDR	Load Constant	Production Constant	Offset (kWh)	%RMSE	MAPE
Toronto	58%	1.462	-0.218	-53	1.678%	-0.897%
Calgary	54%	1.462	-0.262	-49	1.674%	-0.686%
Vancouver	65%	1.462	-0.200	-35	0.744%	-0.246%
Los Angeles	32%	1.462	-0.283	-108	3.629%	-2.227%

It is theorized that the predictive model could work for any target duration provided the mean production and consumption values are calculated accordingly. However,

further investigation is required to validate this hypothesis as the diurnal pattern of PV production may skew model repeatability with non-compatible target durations.

Future Work

Continued efforts on this topic should endeavour to develop more thorough understanding of the mechanisms influencing predictive model coefficients. An important step would be to include a load model that is more representative of actual building performance than the approximation applied herein. This addition would naturally lend to exploring variability consumption dependence according to distribution of consumption data. Effects of round-trip efficiency should also be explored.

Once a more robust understanding of model coefficients is developed, prediction error may be evaluated over a broader range of conditions. The model may also be tested for its relevance at target durations other than 24 hours.

A final interesting step might be to alter the outage simulations to extend beyond battery depletion allowing an analysis of the system's ability to regain temporary charge and function under favourable solar conditions.

Conclusion

Microgrids are a technology of increasing interest worldwide as they offer a variety of value propositions. These range across energy impendence and resiliency to economics and finance in a transactional energy market. Current tools available for modelling and design of microgrids are generally limited in their scope.

This work presents a modelling framework to evaluate the outage performance of a grid connected, building level microgrid consisting of photovoltaic generation, battery storage and critical load. The modelling framework is applied to a broad design space for a subject microgrid. Analysis of the design space yields optimal ranges of battery capacity in both economic and performance-based contexts.

Sensitivity analysis indicates that optimal battery size can be predicted for a given microgrid design as a function of dependencies observed on mean production and consumption over the target duration of load support. A multiple linear regression model is employed to facilitate this prediction and shows promising repeatability with overall MAPE of -1.01%. If further validated, the model may hold value to the microgrid industry in improving and expediting design practices for resilience and off-grid applications.

References

Ahamed, M. H., Dissanayake, U. D., De Silva, H. M., Kumara, H. R., & Lidula, N. W. (2016). Designing and simulation of a DC microgrid in PSCAD. *2016 IEEE International Conference on Power System Technology (POWERCON)* (pp. 1-6). Wollongong, NSW: IEEE.

Andrews, R. W., Pollard, A., & Pearce, J. M. (2013). The effects of snowfall on solar photovoltaic performance. *Solar Energy, 92*, 84-97.

BEW Engineering. (2013). *Performance Model Evaluation.* DNV GL.

Byrne, R. H., Nguyen, T. A., Copp, D. A., Chalamala, B. R., & Gyuk, I. (2017). Energy Management and Optimization Methods for Grid Energy Storage Systems. *IEEE Access, 6*, 13231-13260.

Cui, Y., & Liu, N. (2016). Emergency energy management strategy for commercial building microgrid consisting of PV and energy storage. *2016 IEEE 11th Conference on Industrial Electronics and Applications (ICIEA)* (pp. 2049-2054). Hefei, China: IEEE.

Hirose, K., Shimakage, T., Reilly, J. T., & Irie, H. (2013). *The Sendai Microgrid operational Experience in the Aftermath of the Tohoku Earthquake.* Kawasaki: New Energy and Industrial Technology Development Organization.

Kumar, Y. V., & Bhimasingu, R. (2014). Optimal Sizing of Microgrid for an Urban Community Building in South India using HOMER. *2014 IEEE International Conference on Power Electronics, Drives and Energy Systems.* Mumbai.

Leadbetter, J., & Swan, L. (2012). Battery storage system for residential electricity peak demand shaving. *Energy & Buildings, 55*, 685-692.

Meteotest. (2019). *TMY# (NREL & DWD)*. Retrieved November 2019, from https://meteonorm.com/en/typical-meteorological-years

Rosewater, D. M., Copp, D. A., Nguyen, T. A., Byrne, R. H., & Santoso, S. (2019). Battery Energy Storage Models for Optimal Control. *IEEE Access, 7*, 178357-178391.

Schimpe, M., Naumann, M., Truong, N., Hesse, H. C., Santhanagopalan, S., Saxon, A., & Jossen, A. (2018). Energy efficiency evaluation of a stationary lithium-ion battery container storage system via electro-thermal modelling and detailed component analysis. *Applied Energy, 210*, 211-229.

Tsikalakis, A. G., & Hatziargyriou, N. D. (2011). Centralized Control for Optimizing Microgrids Operation. *2011 IEEE Power and Energy Society General Meeting.* Detroit.

Zimmerle, D., & Manning, D. T. (2017). Optimizing rural village microgrids to provide affordable and reliable renewable electricity in developing countries. *2017 IEEE Global Humanitarian Technology Conference (GHTC)* (pp. 1-6). San Jose, CA: IEEE.